AFRL-RX-WP-TP-2010-4056

MICROSTRUCTURAL CHARACTERIZATION OF FOIL-GAGE HAYNES® 230® (PREPRINT)

W.J. Porter, III and K. Li

University of Dayton Research Institute

R. J. Morrissey and Reji John

Metals Branch
Metals, Ceramics & NDE Division

JANUARY 2010

Approved for public release; distribution unlimited.

See additional restrictions described on inside pages

STINFO COPY

AIR FORCE RESEARCH LABORATORY
MATERIALS AND MANUFACTURING DIRECTORATE
WRIGHT-PATTERSON AIR FORCE BASE, OH 45433-7750
AIR FORCE MATERIEL COMMAND
UNITED STATES AIR FORCE

REPORT DOCUMENTATION PAGE

Form Approved
OMB No. 0704-0188

The public reporting burden for this collection of information is estimated to average 1 hour per response, including the time for reviewing instructions, searching existing data sources, gathering and maintaining the data needed, and completing and reviewing the collection of information. Send comments regarding this burden estimate or any other aspect of this collection of information, including suggestions for reducing this burden, to Department of Defense, Washington Headquarters Services, Directorate for Information Operations and Reports (0704-0188), 1215 Jefferson Davis Highway, Suite 1204, Arlington, VA 22202-4302. Respondents should be aware that notwithstanding any other provision of law, no person shall be subject to any penalty for failing to comply with a collection of information if it does not display a currently valid OMB control number. **PLEASE DO NOT RETURN YOUR FORM TO THE ABOVE ADDRESS**.

1. REPORT DATE *(DD-MM-YY)*	2. REPORT TYPE	3. DATES COVERED *(From - To)*
January 2010	Journal Article Preprint	01 January 2010 – 31 January 2010

4. TITLE AND SUBTITLE
MICROSTRUCTURAL CHARACTERIZATION OF FOIL-GAGE HAYNES® 230® (PREPRINT)

5a. CONTRACT NUMBER
FA8650-04-C-5200

5b. GRANT NUMBER

5c. PROGRAM ELEMENT NUMBER
62102F

6. AUTHOR(S)
W.J. Porter, III and K. Li (University of Dayton Research Institute)
R. J. Morrissey and Reji John (AFRL/RXLM)

5d. PROJECT NUMBER
4347

5e. TASK NUMBER
RG

5f. WORK UNIT NUMBER
M02R3000

7. PERFORMING ORGANIZATION NAME(S) AND ADDRESS(ES)
University of Dayton Research Institute
Dayton, OH 45469-0020

Metals Branch (AFRL/RXLM)
Metals, Ceramics & NDE Division
Materials and Manufacturing Directorate
Wright-Patterson Air Force Base, OH 45433-7750
Air Force Materiel Command, United States Air Force

8. PERFORMING ORGANIZATION REPORT NUMBER

9. SPONSORING/MONITORING AGENCY NAME(S) AND ADDRESS(ES)
Air Force Research Laboratory
Materials and Manufacturing Directorate
Wright-Patterson Air Force Base, OH 45433-7750
Air Force Materiel Command
United States Air Force

10. SPONSORING/MONITORING AGENCY ACRONYM(S)
AFRL/RXLMN

11. SPONSORING/MONITORING AGENCY REPORT NUMBER(S)
AFRL-RX-WP-TP-2010-4056

12. DISTRIBUTION/AVAILABILITY STATEMENT
Approved for public release; distribution unlimited.

13. SUPPLEMENTARY NOTES
Journal article submitted to *Materials Science and Engineering A.* PAO Case Number: 88ABW-2009-4298; Clearance Date: 05 Oct 2009. The U.S. Government is joint author of this work and has the right to use, modify, reproduce, release, perform, display, or disclose the work.

14. ABSTRACT
The microstructures of foil-gage Haynes 230 with thicknesses of 125 and 500 μm (5 and 20 mils, respectively) were characterized using optical, scanning electron (SEM) and electron backscattered diffraction (EBSD) microscopy. The average γ grain size was shown to decrease with foil thickness due to increased plastic deformation and grain recrystallization. Strings of carbides oriented parallel to the rolling direction and located within the equiaxed gamma grains were observed. Room temperature tensile tests revealed a Hall-Petch effect with increasing yield strength associated with decreasing gamma grain size. Tensile properties were very similar between longitudinal and transverse specimens of each thickness. Fractography of the tensile specimens revealed evidence of significant plasticity, localized grain boundary tearing and large carbide fracture for each thickness and orientation.

15. SUBJECT TERMS
grain size, recrystallization, foil-gage, Haynes 230

16. SECURITY CLASSIFICATION OF:			17. LIMITATION OF ABSTRACT:	18. NUMBER OF PAGES	19a. NAME OF RESPONSIBLE PERSON (Monitor)
a. REPORT	b. ABSTRACT	c. THIS PAGE			Reji John
Unclassified	Unclassified	Unclassified	SAR	24	19b. TELEPHONE NUMBER *(Include Area Code)* N/A

Standard Form 298 (Rev. 8-98)
Prescribed by ANSI Std. Z39-18

Microstructural Characterization of Foil-gage Haynes® 230®

W. J. Porter, III[1], K Li[1], R. J. Morrissey and R. John

U. S. Air Force Research Laboratory, Materials and Manufacturing Directorate,
AFRL/RXLMN, Wright-Patterson AFB, OH 45433-7817
[1]University of Dayton Research Institute, Dayton, OH 45469-0020

Abstract

The microstructures of foil-gage Haynes 230 with thicknesses of 125 and 500 μm (5 and 20 mils, respectively) were characterized using optical, scanning electron (SEM) and electron backscattered diffraction (EBSD) microscopy. The average γ grain size was shown to decrease with foil thickness due to increased plastic deformation and grain recrystallization. Strings of carbides oriented parallel to the rolling direction and located within the equiaxed gamma grains were observed. Room temperature tensile tests revealed a Hall-Petch effect with increasing yield strength associated with decreasing gamma grain size. Tensile properties were very similar between longitudinal and transverse specimens of each thickness. Fractography of the tensile specimens revealed evidence of significant plasticity, localized grain boundary tearing and large carbide fracture for each thickness and orientation.

Key words: grain size, recrystallization, foil-gage, Haynes 230

Introduction

Haynes 230is a solid-solution- and carbide-strengthened nickel-based superalloy noted for its excellent high-temperature strength, resistance to oxidizing environments, microstructural stability, and a low coefficient of thermal expansion (CTE) [1]. Haynes 230 is employed in a number of thermally- and chemically-aggressive environments including turbine engine combustor cans, transition ducts and flameholders, in chemical plant heat exchangers and bellows, and as burner flame shrouds and heat treating baskets in the industrial heating industry [2]. Another promising application for alloys such as Haynes 230 is in metallic-based thermal protection systems (TPS) for utilization in advanced aerospace systems such as the military Space Operations Vehicle [3]. Reliable design of these structures require basic understanding of material behavior under simulated service conditions While there are a significant number of publications relative to Haynes 230 in the bar, plate and sheet form [1, 4-6], there is a paucity of publications dealing specifically with foil-gage materials. The foil-gage materials are especially important for metallic honeycomb structures envisioned for TPS application [7,8].

The objective of the present work was to characterize the foil microstructures and investigate the relationship between foil-gage thickness and γ grain size, specimen orientation and room temperature tensile behavior.

Material and Experimental Procedure

The typical microstructure in Haynes 230is composed of three primary phases: a gamma (γ) matrix phase (face centered cubic) and two carbide phases. The matrix γ phase generally has an

equiaxed morphology following high temperature annealing due to full recrystallization. The carbides are present in the form of small grain boundary chromium carbides with the formula $M_{23}C_6$ [9] and a pronounced primary tungsten carbide present in strings parallel to the rolling direction and having the formula M_6C [9].

The Haynes 230 materials were supplied in their foil-gage form by Elgiloy Specialty Metals (Elgin, IL, USA). The nominal composition (wt. %) of the Haynes 230 is given in Table 1 [2].

All metallographic samples were mechanically polished using standard metallographic techniques. The electron backscattered diffraction (EBSD) data was collected using the following scanning electron microscope (SEM) settings: specimen voltage of 20kV, probe current of 10 nA, and 0.5 μm per scanning step. Following EBSD scanning, the specimens were chemically etched to enhance optical and secondary electron microscopy efforts. The following etching sequence was utilized: submerge specimen in hydrochloric acid (HCl) for 10 sec; rinse in methanol; submerge sample in a solution of 1% bromine in methanol for 20 or 40 seconds; rinse sample in methanol and dry. Transverse and longitudinal cross-sections of each foil were investigated.

Tensile tests were performed at room temperature using a loading rate of 0.045mm/s on a servohydraulic machine. Deformation was monitored using standard strain gages on both sides of the specimen. Average strain data are reported in this paper. Longitudinal and transverse specimens were investigated. Details of the foil-gage specimen tensile testing techniques can be found in [10].

Results and Discussion

As-received Material

All of the foil-gage material used in this study came from the same initial ingot heat. The actual chemistry for this ingot is shown in Table 1. It should be noted that the nominal values for the cobalt, iron and boron represent 'not to exceed' value and that the measured values from the ingot in this study meet this standard.

Material representing two foil thicknesses, 125 and 500μm (5 and 20 mils, respectively), were investigated. The foils were received in 33 cm wide rolls (13 in.) with each weighing 11.34 kilograms (25 pounds). A typical etched optical image from a 500 μm thick longitudinal specimen is shown in Figure 1. The grain boundaries and twins highlight the equiaxed nature of the microstructure. The strings of carbides, running from left to right, are also apparent.

Figure 2 shows low magnification, backscattered electron images for longitudinal and transverse cross sections of each material. The 'stringered' nature of the large tungsten carbide particles is apparent in the longitudinal images. The uniform distribution of these large carbides throughout the cross section of each foil is shown in the transverse images. The volume percent of the tungsten carbide particles (M_6C) was measured to be approximately 3% for each foil thickness. Volume measurements of the grain boundary chromium carbides ($M_{23}C_6$) were not made due to difficulty in imaging sufficient quantities of this phase.

The fractured nature of many of the large tungsten carbides from each foil thickness is highlighted in Figure 3. These particles are believed to be fractured during the rolling processes necessary to manufacture the foil. The voids or dark areas associated with the fractured carbides were likely formed by loss of carbide-related debris during specimen preparation. The magnitude and general appearance of the fractured particles is similar for each foil thickness investigated and suggests that the fracture events occurred early in the foil processing scheme.

The submicron, chromium-rich $M_{23}C_6$ carbides are shown in Figure 4. These carbides are isolated to grain boundary regions and serve to strengthen the grain boundary and hinder grain boundary sliding [11, 12].

Electron backscattered diffraction (EBSD) data was used to generate the inverse pole figure (IPF) maps shown in Figure 5. Each IPF map reveals an array of randomly distributed crystallographic orientations. The random nature of the grain orientations is due to the recrystallization brought on by the repeated upsetting and reheating associated with the foil making process [13]. The IPF maps also clearly reveal the annealing twins present throughout the foils.

The EBSD data was used to calculate the grain sizes for each foil. A comparison of the grain size for each foil is shown in Figure 6 where the calculated grain diameter is plotted against the area fraction. Not surprisingly, the 125μm material exhibited a finer grain size than the 500 μm due to the additional work input to the material to manufacture a thinner gage section product.

Room Temperature Tensile Testing and Fractography

The tensile results from room temperature longtiudinal and transverse specimens are shown in Figure 7 (a) and (b), respectively. Figure 8 is a close-up look at the low strain response of the same results shown in Figure 7. A summary of the tensile data is shown in Table 2. The finer grained, 125μm material exhibited higher yield and ultimate tensile strength than its coarser grained 500 μm counterpart. This result is not unexpected and is consistent with the theory of Hall-Petch or grain boundary strengthening where grain boundaries act as impediments to dislocation movement resulting in higher yield properties [14, 15].

For each material, the transversely oriented material exhibits a slightly higher yield strength than the longitudinally oriented material while, conversely, the ultimate tensile strength is higher in the longitudinal specimens for each. The modulus values for each of the specimens are very consistent and seem to indicate that specimen orientation, in particular, the distribution of the large MC_6 tungsten carbides, do not seem to affect the elastic response of the material. These properties are consistent with data from the manufacturer of the alloy [2].

The fracture surfaces of the longitudinal and transverse specimens for each foil thickness are shown in Figures 9 and 10. Widespread plasticity is evidenced in all of the images. Also, all of the higher magnification images reveal very localized regions exhibiting brittle type fracture. These regions correspond to the MC6 tungsten carbide particles found throughout the material. Figures 9(b,c and e,f) and10 (b,c and e,f) best highlight this feature. The secondary electron images (9(b) and (e)) and 10(b) and(e)) reveal the localized brittle features while the

backscattered electron images (9(c) and (f)) and 10(c) and(f)) reveal these features as tungsten carbide particles. As in the micrographs shown in Figure 2 and 3, the bright contrast of the tungsten carbides is indicative of a large difference in elemental density (i.e Z-contrast) between the matrix material and the tungsten-rich carbides.

The longitudinal and transverse specimens for each foil thickness have very similar characteristics. For example, the fracture surfaces of each of the transverse specimens reveal the stringers of carbides seen in the longitudinal metallographic images and conversely, the carbides are evenly distributed across the fracture surfaces of the longitudinal specimens. This is expected as the test specimen orientations will reveal features normal to their complementary metallographic specimens.

The higher magnification fracture surfaces expose many carbide particles that appear to be fractured. This is consistent with the many fractured carbides encountered in the metallographic specimens. The relatively low strength of the matrix material should not have the ability to impart the damage required to fail the carbides and reinforces the idea the carbide particles were damaged during the foil rolling process.

Conclusions

The microstructure and room temperature tensile properties of foil-gage Haynes 230 was investigated. Two foil thicknesses, 125 and 500 μm, were characterized to determine the similarities and differences, in terms of microstructural appearance and tensile properties, possessed by each. Optical and scanning electron microscopy, including electron backscattered diffraction, was employed for the microstructural comparison. The fully-recrystallized nature of the Haynes 230 foils yielded very similar microstructure features regardless of material thickness and orientation. The primary microstructural differences included stringered carbides in the longitudinal specimens versus the widely distributed carbides in the transverse specimens due to the effects of rolling and a slight difference in grain size. The 125μm material was found to have a finer grain size than the 500μm material due to the additional mechanical work required to get to the thinner gage width. The 125μm material exhibited higher strengths than the 500μm material, consistent with the Hall-Petch or grain boundary strengthening theories. Fractography of the room temperature tensile surfaces showed distinct similarities for a given orientation regardless of specimen thickness.

Acknowledgments

This work was performed at the Air Force Research Laboratory, AFRL/RXLMN, Materials and Manufacturing Directorate, Wright-Patterson Air Force Base, OHre. Kezhong Li and W. John Porter, III were supported under AF Contract No. FA8650-09-D-5223. The authors gratefully acknowledge the assistance of Phil Blosser and Mark Ruddell in conducting the tensile tests and technical discussions with Dr. Dennis Buchanan.

References

1 Y.L. Lu,, P.K. Liaw, G.Y. Wang, M.L. Benson, S.A. Thompson, J.W. Blust, P.F. Browning, A.K. Bhattacharya, J.M. Aurrecoechea, D.L. Klarstrom, *Materials Science and Engineering A* 397 (2005) 122–131.

2 Haynes on-line literature, No. H-3000H, Haynes®230® Alloy Brochure, www.haynesintl.com, 2004.

3 C.L. Clay, *Journal of Aircraft*, Vol. 41, No. 5, September–October (2004) 978-985.

4 D.L. Klarstrom, US Patent 4,476,091 (1982).

5 Y.L. Lu, L.J. Chena, P.K. Liaw, G.Y. Wang, C.R. Brooks, S.A. Thompson, J.W. Blust, P.F. Browning, A.K. Bhattacharya, J.M. Aurrecoechea, D.L. Klarstrom, *Materials Science and Engineering A* 429 (2006) 1–10.

6 A. Thakur, K. S. Vecchio, and S. Nemat-Nasser, *Metallurgical And Materials Transactions A* Volume 27A (July 1996) 1739.

7 M.L. Blosser, C.J. Martin, K. Daryabeigi, C.C. Poteet, Reusable metallic thermal protection systems development, in: Proceedings of the 3rd European Workshop on Thermal Protection Systems, ESTEC, March 25–27, 1998, pp. 165–176.

8 M.L. Blosser *et al.*, *Journal of Spacecraft and Rockets* **41** (2) (2004), pp. 183–194.

9 H.M. Tawancy, D.L. Klarstrom & M.F. Rothman, *J. Met*. 36(1984) 58-62.

10 Morrissey, R.M., John, R., Ruddell, P. Blosser, "Test System For Foil-gage Metals", Submitted for publication, October 2009.

11 Donachie, M.J., Donachie, S.J., (2002). Superalloys. A Technical Guide. 2nd edition. Materials Park: ASM International.

12 Davis, J.R., (1997). Heat Resistant Materials Materials Park: ASM International.

13 R.D. Doherty, D.A. Hughes, F.J. Humphreys, J.J J.onas, D. Juul Jenson, M.E. Kassner, W.E. King, T.R. McNelley, H.J. McQueen, A.D. Rollett , *Materials Science and Engineering* **A238** (1997) 219–274.

14 E.O. Hall, *Proc. Phys. Soc. London B* **64** (1951), p. 747.

15 N.J. Petch, *J. Iron Steel Inst.* **174** (1653), p. 25.

Table 1: Nominal [2] and actual composition (wt%) of the Haynes 230 used in this study.

	Ni	Cr	W	Mo	Fe	Co	Mn	Si	Al	C	La	B
Nominal	57**	22	14	2	<3*	<5*	0.5	0.4	0.3	0.1	0.02	<0.015*
This study (ingot chem.)	59.625	22.546	14.179	1.299	1.245	0.224	0.544	0.376	0.381	0.108	0.015	0.002

*max **as balance

Table 2: Room temperature tensile results for foil-gage longitudinal and transverse specimens.

Foil Thickness	Orientation	E (GPa)	0.2% YS (MPa)	UTS (MPa)	El (%)
125 μm	Long.	208	564	989	33.1
	Trans.	210	600	954	36.4
500 μm	Long.	210	502	946	41.0
	Trans.	221	506	849	31.2

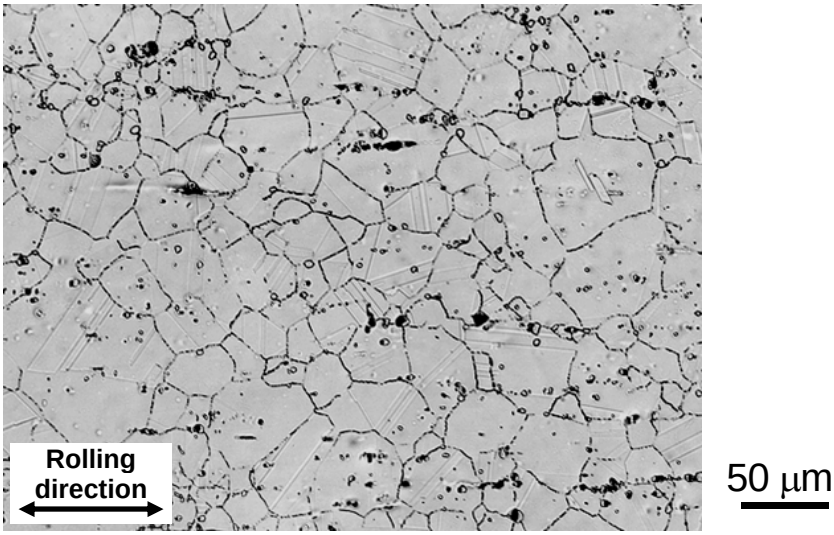

Fig. 1 - Typical optical micrograph of etched, longitudinally-oriented Haynes230 highlighting grain boundaries, extensive twinning and presence of tungsten carbide strings.

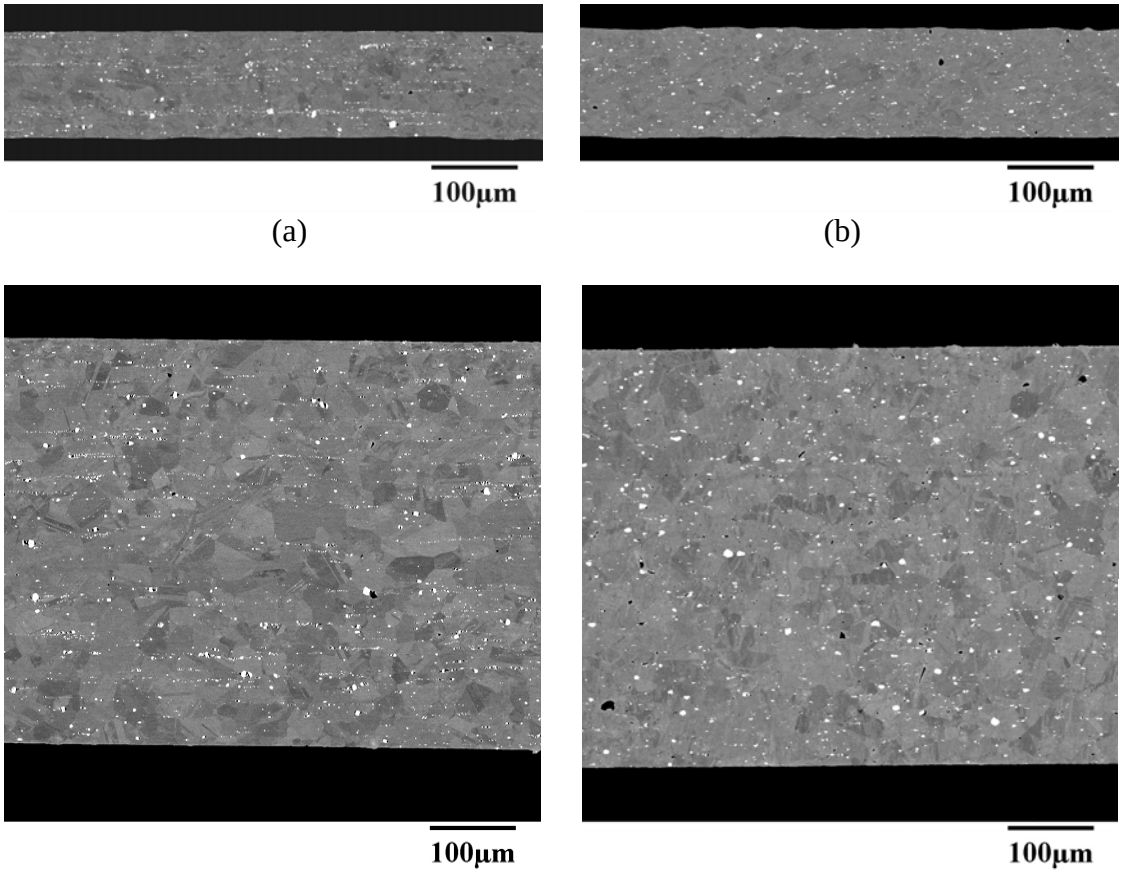

Figure 2 –Backscattered electron images, low magnification, showing strings of tungsten carbide particles parallel to sample surface in the longitudinal orientation for each foil-gage thickness in (a) 125µm and (c) 500µm, and generally uniform distribution throughout the transverse cross sections in (b) 125µm and (d) 500µm.

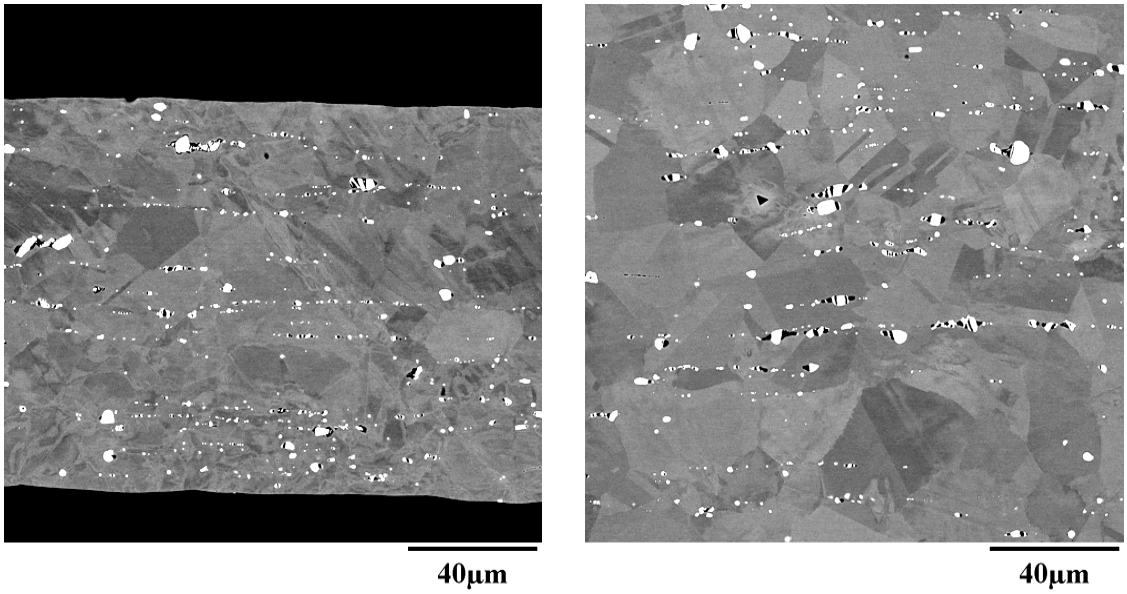

(a) (b)

Figure 3 – Backscattered electron images of (a) 125µm and (b) 500µm thick material revealing fractures in large tungsten carbide particles most likely brought on by foil rolling processes.

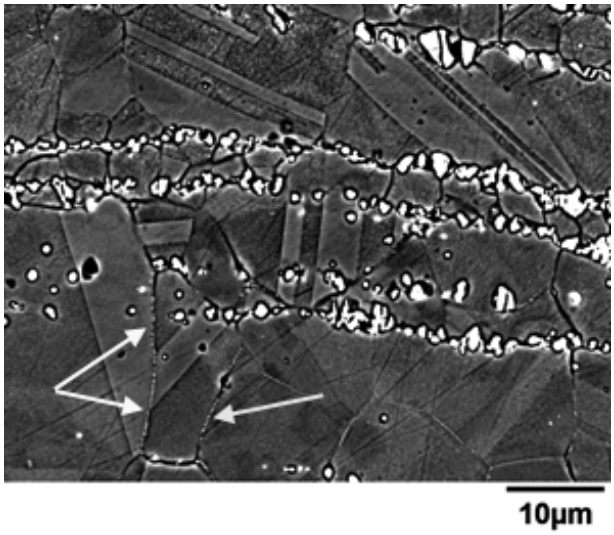

Figure 4 – Backscattered electron image highlighting the small chromium–rich carbides ($M_{23}C_6$), identified by the white arrows, isolated at grain boundaries. Note the presence of extensive twinning throughout the image.

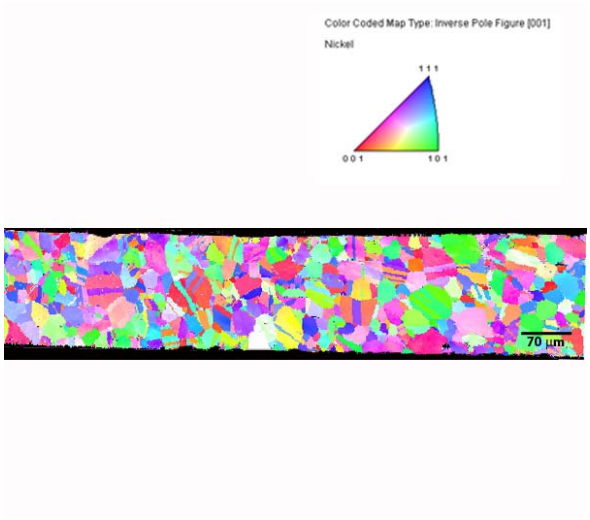

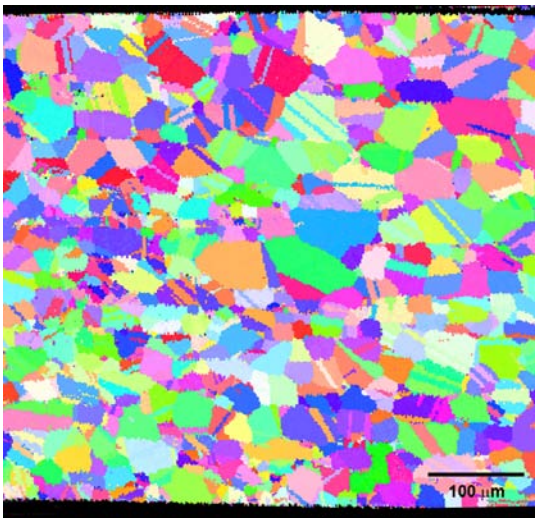

(a) (b)

Figure 5 – EBSD data shown as inverse pole figure (IPF) maps revealing general absence of any crystallographic texture due to recrystallization in (a) 125 μm and (b) 500 μm thick foils. Longitudinal orientations are shown; transverse data is indistinguishable from longitudinal, again due to recrystallized nature of the microstructure.

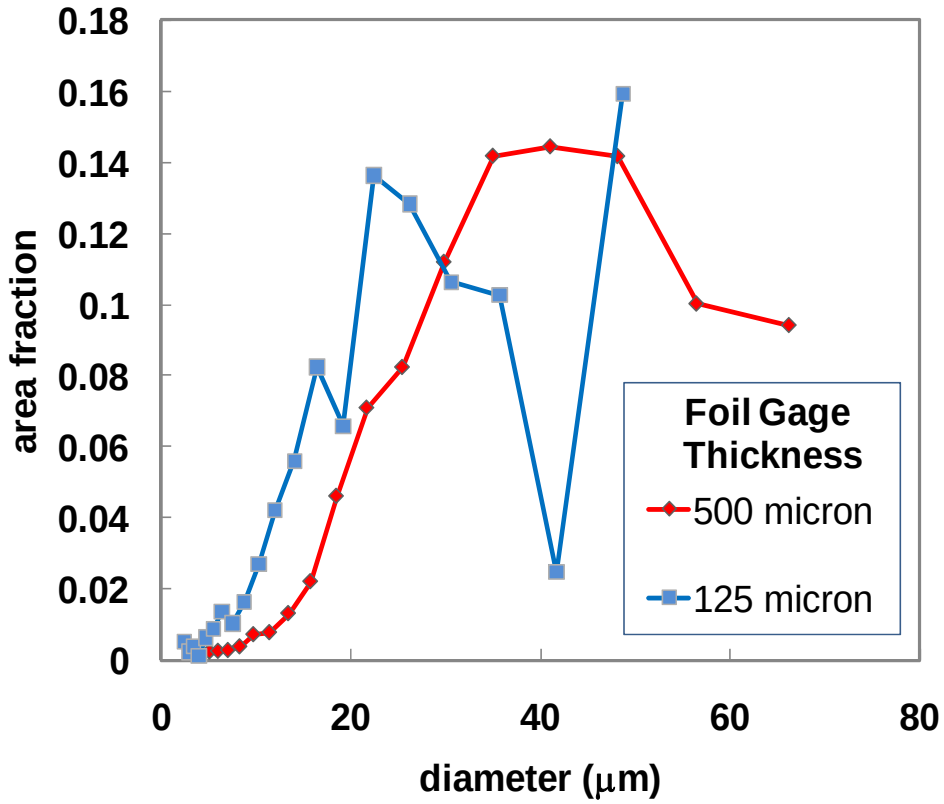

Figure 6 - Comparison of the grain size for both the 125 and 500 μm thick foils.

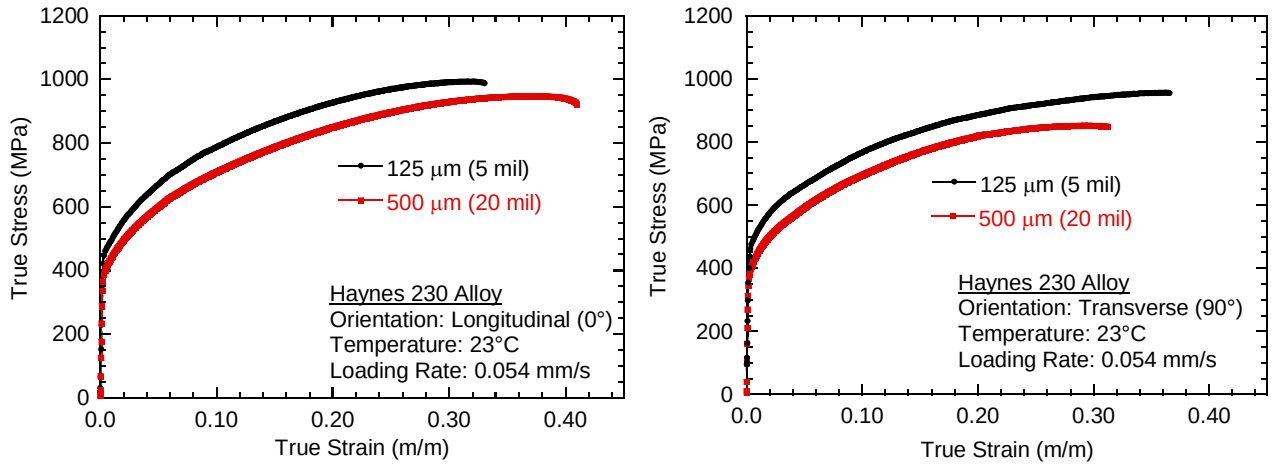

(a) (b)

Figure 7: Comparison of room temperature tensile response as a function of specimen thickness of (a) longitudinal and (b) transverse specimens. Yield stress is shown to increase with decreasing grain size and specimen thickness.

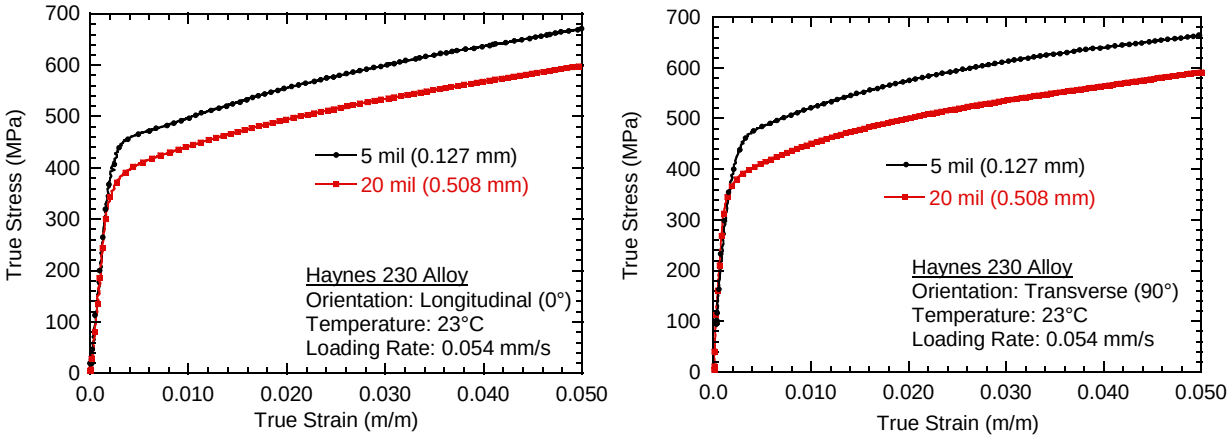

Figure 8: Comparison of low strain room temperature tensile response as a function of specimen thickness of (a) longitudinal and (b) transverse specimens.

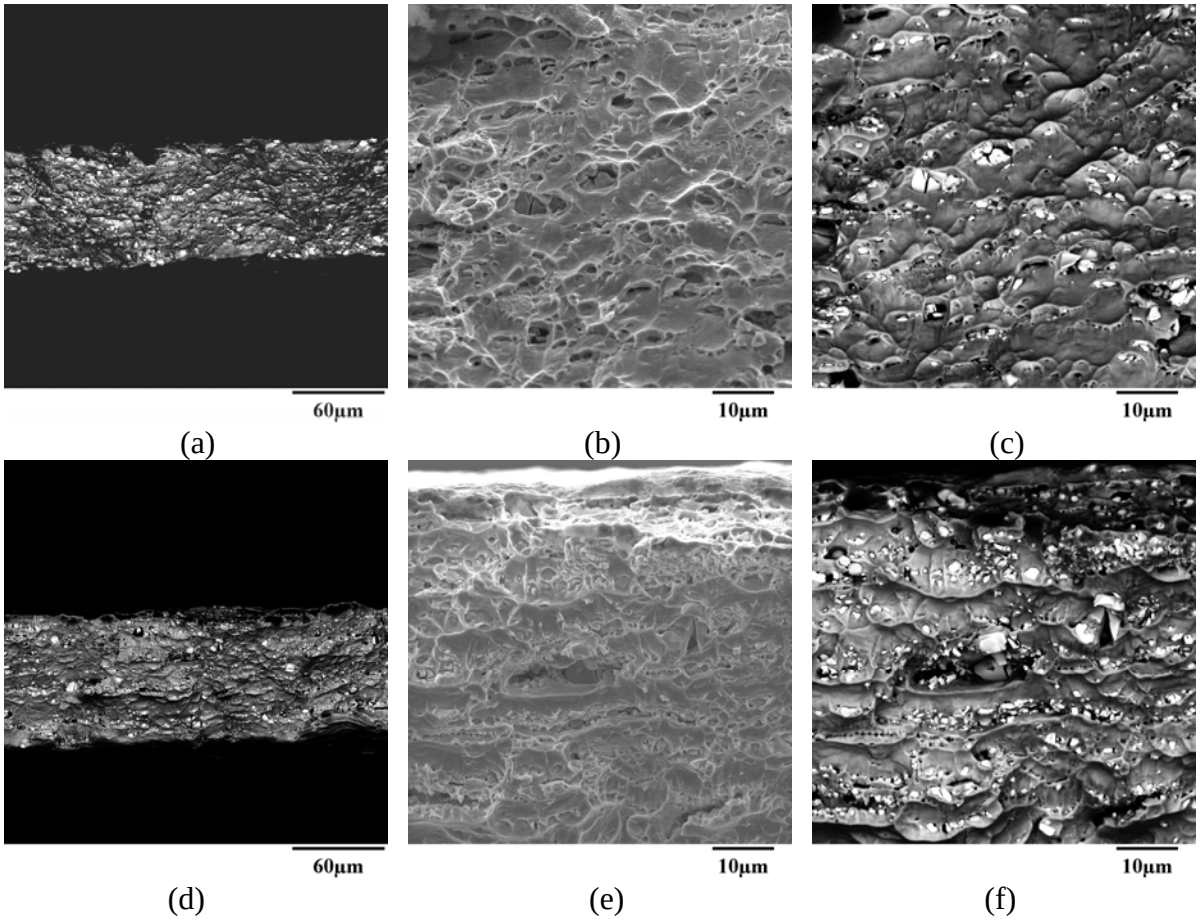

Figure 9: SEM images of a 125µm thick longitudinal (a-c) and transverse (d-f) fracture surfaces. (a,c) Low magnification views of fracture surfaces showing widespread plastic deformation, (b, e) high magnification images revealing gross plastic deformation with intermittent brittle type failure areas corresponding to carbide particles, and (c, f) backscattered image of (b) showing presence of broken carbide particles (light contrast) throughout fracture surface. Note the presence of MC6 carbides in (f).

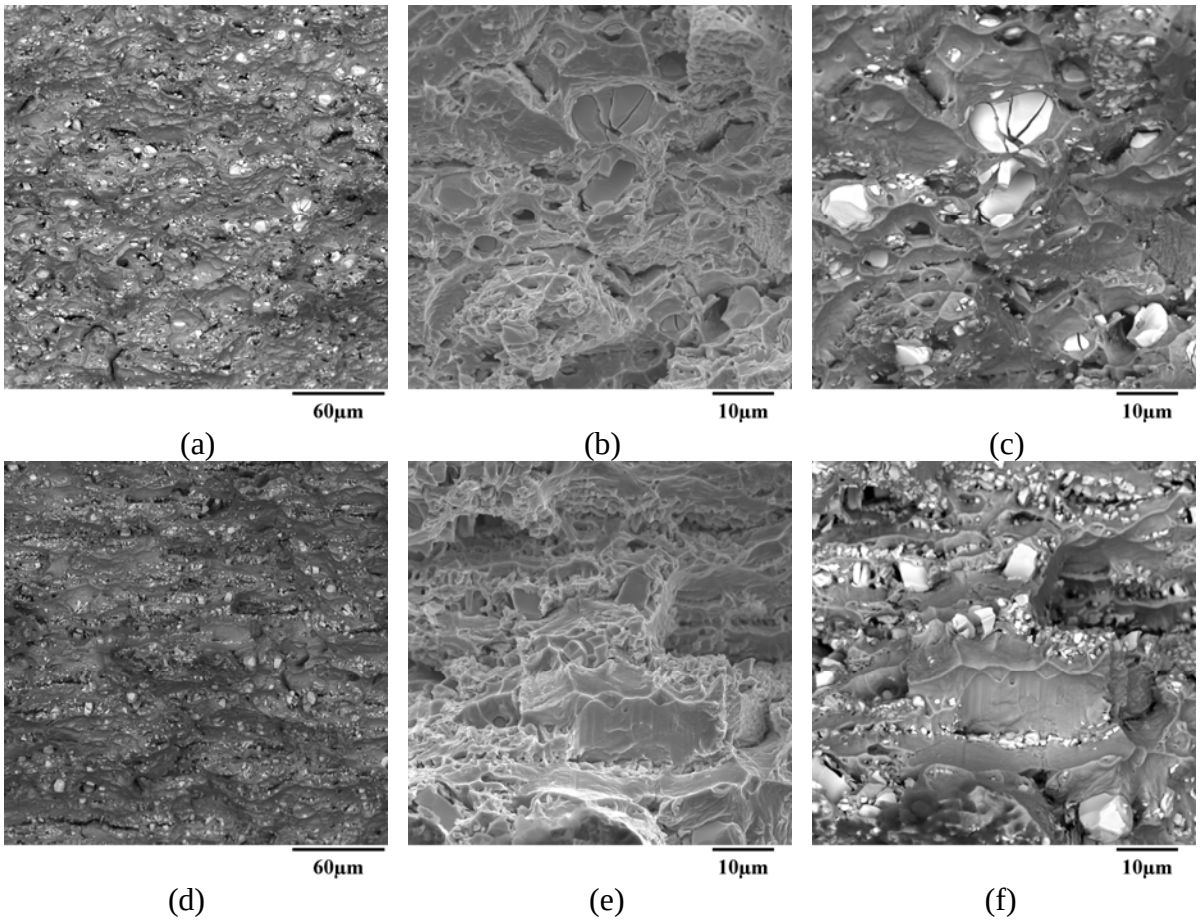

Figure 10: SEM images of a 125µm thick longitudinal (a-c) and transverse (d-f) fracture surfaces. (a,c) Low magnification views of fracture surfaces showing widespread plastic deformation, (b, e) high magnification images revealing gross plastic deformation with intermittent brittle type failure areas corresponding to carbide particles, and (c, f) backscattered image of (b) showing presence of broken carbide particles (light contrast) throughout fracture surface. Note the presence of MC6 carbides in (f).